RSC Advances

PAPER

View Article Online
View Journal | View Issue

Cite this: *RSC Adv.*, 2026, **16**, 11988

Amide-linked hole transporting material for solid-state dye-sensitised solar cells

Amy Neild, [a] Owen Woodford,[a] Pablo Docampo[b] and Elizabeth A. Gibson *[a]

This paper reports the first use of an amide-based hole transport material in a solid-state dye-sensitised solar cell. A substantial improvement in solar cell efficiency from 0.04 to 2.26% was achieved through prolonged oxidation in air and light soaking for the amide-based hole-transporting mediator, TPABT. Time-resolved spectroscopic studies show that the oxidation state and additive concentration alter the charge-transfer and regeneration kinetics, which are consistent with the time-dependent changes in device properties. Our study shows that, if the oxidation state and doping are carefully controlled, TPABT-based hole transport materials could serve as a viable, cost-effective alternative to Spiro-OMeTAD, the conventional yet expensive hole-transporting material widely used in emerging photovoltaics.

Received 3rd December 2025
Accepted 16th February 2026

DOI: 10.1039/d5ra09351a

rsc.li/rsc-advances

Introduction

Hybrid solar cells, including perovskite solar cells (PSC), dye-sensitized solar cells (DSSCs), and organic photovoltaics (OPVs) are printable/solution-processable photovoltaic (PV) technologies, often composed of earth-abundant elements.[1–3] This allows for minimal, cost-effective manufacturing infrastructure compared to traditional silicon-based PV. The operational lifetime of these devices is primarily limited by (i) the durability of the light-absorbing and charge-transport layers, (ii) the integrity of interfaces within the device architecture, and (iii) the resistance to degradation at the electrical contacts.

Current research efforts in hybrid PV have primarily focused on optimizing the light-absorbing layers, leading to major advances in device efficiency. For instance, in organic PV, the development of non-fullerene charge transport materials (CTMs) has been transformative, as these CTMs now not only facilitate charge transfer but also actively contribute to light absorption.[4,5] Despite these advancements, charge extraction layers in other hybrid devices have attracted comparatively less attention. Large knowledge gaps still exist for these materials and their development lags behind effort dedicated to light absorbing materials. In fact, present-day state-of-the-art devices still often employ CTMs developed over a decade ago. These materials can be the most expensive component in hybrid PVs.[6]

The most well-known hole-transport material (HTM) for solid-state dye-sensitized solar cells (ssDSSCs) and PSCs is 2,2′,7,7′-tetrakis-(*N*,*N*-di-4-methoxyphenyl amino)-9,9′-spirobifluorene (Spiro-OMeTAD) (Fig. 1).[7,8] Spiro-bifluorene is an expensive starting material and the cost of manufacturing Spiro-OMeTAD is estimated to be ~$90 g^{-1}.[9] This significant contribution to the total device cost, coupled with the tedious synthesis, hinders the commercialisation of devices that contain the material. Other proposed alternatives occasionally compete performance-wise with Spiro-OMeTAD, but do not address the limitation when they are also synthesised in multi-step procedures with extensive product purification.[10,11]

While spiro-OMeTAD remains the benchmark CTM for hybrid solar cells, it suffers from intrinsic instability problems and low carrier mobility.[12] Adachi *et al.* call it the "Achilles heel".[13] The inclusion of additives, such as lithium bis-trifluoromethanesulfonimidate (LiTFSI) and 4-*tert*-butylpyridine (*t*BP) in relatively high concentrations, to the HTM is essential to achieve sufficient conductivity and for optimal energy alignment at the interfaces.[14–17] Such high concentrations of hygroscopic and volatile dopants can lead to instability.[18] These additives tend to migrate over time. This migration promotes the formation of film defects such as pinholes, accelerating device ageing and degradation.[19] The search for additive-free charge transport materials that combine high performance with stability is an emerging and rapidly growing area of research.[20] However, to date, there is no universally accepted alternative outperforming spiro-OMeTAD in all relevant metrics in practical device operation.[21]

Traditionally, molecular CTMs are designed to maximize hole delocalization across the molecule, commonly through fully conjugated structures. This design paradigm has restricted the exploration of alternative materials and synthetic approaches for many years. Significant progress in ssDSSCs has recently been achieved with the introduction of copper coordination complexes as CTMs. This strategy has resulted in record-

[a]*Energy Materials Laboratory, School of Natural and Environmental Sciences, Newcastle University, Chemistry, Bedson Building, Newcastle upon Tyne, NE1 7RU, UK. E-mail: elizabeth.gibson@newcastle.ac.uk*

[b]*Basque Centre for Materials, Nanostructures and Applications, Leioa 48940, Spain. E-mail: pablo.docampo@bcmaterials.net*

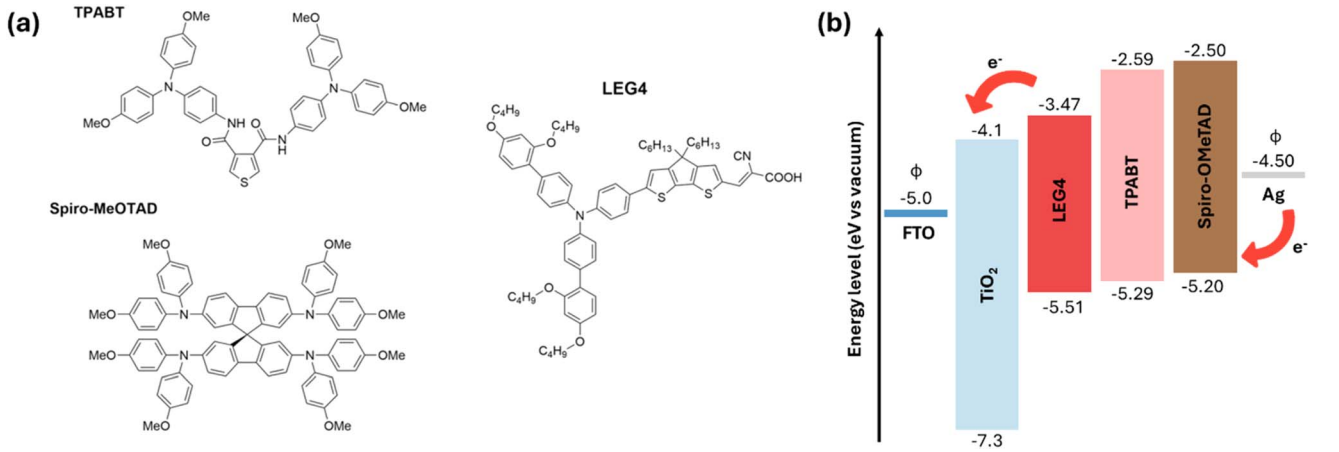

Fig. 1 (a) Structures of Spiro-OMeTAD and TPABT hole transport mediators, and LEG4 organic sensitising dye explored in this work. (b) Energy level diagram of the components in the device.[28,33,34]

breaking device efficiencies exceeding 15% and offers a simpler, more cost-efficient synthesis compared to the widely-used spiro-OMeTAD CTM.[22] Further work is needed to enable scalable manufacturing of ssDSSCs using copper coordination complexes, however.[23,24] X60 has also emerged as a CTM showing high efficiencies of *ca.* 7% synthesised from cheap commercially available starting materials.[25] ssDSSCs that utilise electronically conducting polymers as CTMs have shown excellent operational stability with increased performance over 1000 h.[26]

Recently, a new generation of hole transporting materials has been applied in PSCs, which reach power conversion efficiencies comparable to Spiro-OMeTAD based devices, but are synthesised in a simple, low-cost condensation reaction, under ambient conditions, with water as the only byproduct and no need for catalytic metals.[27] Despite a lack of conjugation through the molecule, when deposited as thin films in PSCs, they demonstrate properties such as fast hole injection rate, reduced interfacial recombination, and improved device stability, while keeping synthesis costs to less than $10 per gram in the lab (costs may decrease if commercialised).[9] It is possible that the intermolecular interactions and close molecular packing lead to good intermolecular orbital overlap and charge transport properties, potentially giving a performance advantage.

TPABT, (N^3,N^4-bis(4-(bis(4-methoxyphenyl)amino)phenyl) thiophene-3,4-dicarboxamide (Fig. 1), has shown promising performance in PSCs.[28] Aromatic amides are attractive hole transporting materials due to their low-cost, metal-free synthesis under mild conditions and straightforward purification. Although non-conjugated amide bonds are typically seen as poor for charge transport, strong intermolecular interactions in bulk materials can compensate by enhancing orbital overlap and improving charge mobility. The shorter hole-hopping distance between molecules results in a good electrical conductivity of $\sim 8 \times 10^{-5}$ S cm^{-1} (*ca.* an order of magnitude less than Spiro-OMeTAD under similar conditions).[29] However, TPABT has a wider bandgap making it more transparent in the visible range of the solar spectrum than Spiro-OMeTAD, which leads to lower parasitic absorption losses.[28] This suggests that TPABT might possess the capability to exceed Spiro-OMeTAD in terms of both performance and cost-effectiveness in a ssDSSC. Transparency is important since, unlike planar PSCs, the HTM is infiltrated into the pores of the mesoscopic structured electrode where it might otherwise compete for light with the dye.

We sought to explore the application of the aromatic amide TPABT (Fig. 1a) as an HTM in ssDSSCs. We chose the organic dye LEG4 (Fig. 1a), which is commercially available, has a high molar extinction coefficient and is one of the most efficient photosensitizers used in ssDSSCs.[30,31] Previously an efficiency of 7.7% was reported by using the organic dye LEG4 with 1,1,2,2-tetrachloroethane (TeCA) doped Spiro-OMeTAD as the HTM.[32] The HOMO of LEG4 is also close in energy to that of TPABT (Fig. 1b). We set out to optimise the concentration of additives for new the HTMs in ssDSSCs, because they are so important for the charge separation and transport processes, however the results were not as initially expected. In freshly prepared devices, the solar cell performance was poor, and it was not possible to observe significant improvements with the different HTM solutions. After prolonged oxidation and light soaking, improvements in performance emerged and trends appeared that were not obvious in PSCs.[28] The ssDSSC configuration enabled us to explore, spectroscopically, the effects of the dopants and our experiments revealed new insight into the effects of additives and ageing on the performance of the new HTM.

Results

Solid-state dye-sensitized solar cells

ssDSSCs were prepared according to the procedure outlined in the SI. LiTFSI and *t*BP were added to chlorobenzene solutions of the HTMs to ensure good conductivity of the deposited film and optimal charge transfer at the TiO_2|TPABT heterojunction. The HTM was applied by spin coating. Following evaporation of the metal contact, the devices were stored overnight, in the dark, in

an air-filled desiccator to allow the HTM to oxidise. We previously found the optimised concentration of Spiro-OMeTAD and additives to be 100 mg ml^{-1} Spiro-OMeTAD, 76 mM *t*BP and 25 mM LiTFSI. We then explored a range of concentrations of additives to improve the properties of TPABT. Firstly, two series (S and T) were tested where the concentration of additives were increased but keeping the ratio of *t*BP : LiTFSI constant (1 : 0.33 for S, 1 : 0.22 for T). Secondly, the *t*BP concentration was fixed at 76 mM, to be consistent with the previously optimised Spiro-OMeTAD recipe, and the concentration of LiTFSI was varied. The concentration of TPABT was kept to 50 mg ml^{-1} for all devices, which was the limit of the TPABT solubility in chlorobenzene.

Current density *vs.* voltage (*J*–*V*) scans were conducted under AM1.5, 100 mW cm^{-2} illumination to investigate how varying the concentration of additives influenced the performance of the devices. While the Spiro-OMeTAD devices performed as expected, the TPABT devices had a lower open-circuit voltage (V_{OC}), despite having a lower HOMO level and built in potential than Spiro-OMeTAD, and were limited by very low short-circuit current density (J_{SC}), fill factor (FF), and power conversion efficiency (PCE). These shortcomings may result from inefficient electron injection into the TiO_2 conduction band, poor hole extraction from the dye to TPABT, or the inherently low conductivity of TPABT. Since LEG4 is effective in Spiro-OMeTAD devices, the issues are most likely due to the properties of the TPABT, and so we continued to optimise further.

The experiments with the first series (S and T) indicated that LiTFSI had a larger influence on device performance than *t*BP (see Table S1) and the optimum concentration of LiTFSI was found to be approx. 75 mM (Fig. 2a and Table 1). This was three times the concentration of LiTFSI required for Spiro-OMeTAD devices, suggesting that the doping affect may differ. For example, differing degrees of hysteresis depending on scan direction were observed, despite the low current densities. Higher additive concentrations, particularly above 75 mM LiTFSI, were found to intensify hysteresis and cause unusual *J*–*V* curve behaviour when scanning from OC to SC, where current declines sharply after reaching a peak rather than plateauing. While most SC to OC scans appeared typical, exceptions like S2 and T3 (where LiTFSI concentration was 76 and 75 mM, respectively, but T3 contained an additional 114 mM *t*BP) exhibited the opposite behaviour at low voltages, with current decreasing steeply as voltage increased (Fig. 2a and Table 1). These observations are typical of hybrid solar cells at intermediate LiTFSI concentrations and have been attributed to ion migration and accumulation, interfacial charge trapping, and changes in surface electric fields.[1,35–37]

A second batch of experiments sought to understand the effects of varying the LiTFSI concentration in more detail, keeping the concentration of *t*BP constant (76 mM, consistent with the optimised concentration used in ssDSSCs employing spiro-OMeTAD). Since *t*BP can shift the conduction band edge of TiO_2 upward in energy (*i.e.*, to a more negative potential), lowering the concentration may enhance electron injection from the sensitized dye into the mesoporous TiO_2.[38,39] Too much *t*BP can also decrease hole conductivity and reduce efficiency, since it decreases the oxidation level of Spiro-OMeTAD, leading to lower current. It can be difficult to interpret these effects, however, since *t*BP has also been found to increase the solubility of LiTFSI in the HTM solution.[40] In the context of ssDSSCs, therefore, this adjustment not only facilitates more efficient charge transfer at the dye|TiO_2 interface but may also improve the J_{SC} and overall device performance by optimizing the driving force for electron injection.[41] The initial results are provided in Table S2 and Fig. 3. Significant hysteresis occurred with around 75 mM LiTFSI, and the *J*–*V* curve characteristics were consistent with the S and T series, despite the lower *t*BP concentration.

While LiTFSI was expected to enhance J_{SC} by lowering the conduction band edge of TiO_2, (accelerating charge injection) and increasing the conductivity of the HTM,[17,28,42] higher concentrations (25–75 mM) reduced both V_{OC} and J_{SC}. This is possibly due to changes in the trap state density, especially deep traps, and enhanced recombination.[42,43] At 100 mM Li-TFSI, no photocurrent was generated, likely due to excessive p-doping and/or ionic accumulation at interfaces and a shift in the band alignment that hinder charge transfer, transport, and collection. TPABT devices show much lower currents than Spiro-OMeTAD under the same additive conditions, further

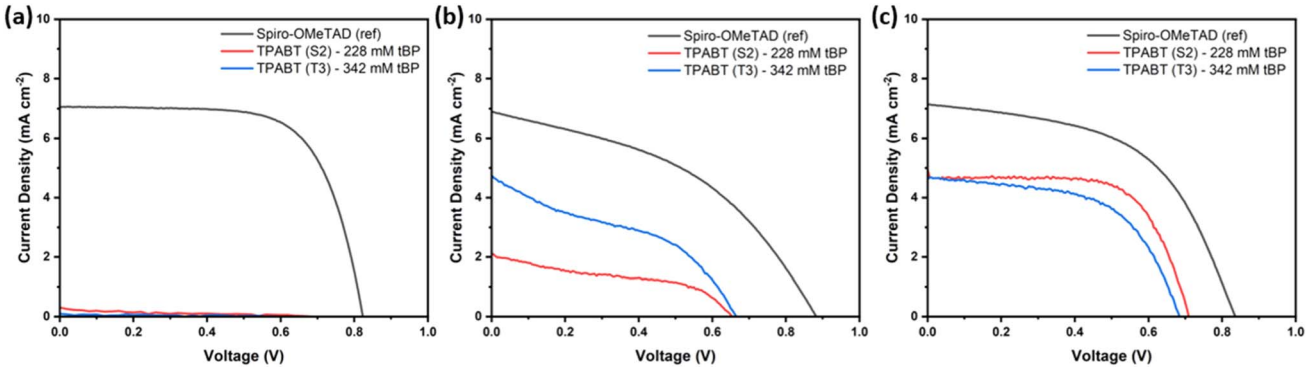

Fig. 2 *J*–*V* curves for the first series of FTO|TiO_2|LEG4|HTM|Ag ssDSSC with TPABT (50 mg ml^{-1} TPABT, 76 mM LiTFSI and 228 mM *t*BP (red), and 75 mM LiTFSI and 342 mM *t*BP (blue)) and Spiro-OMeTAD (25 mM LiTFSI and 76 mM *t*BP and 100 mg ml^{-1} Spiro-OMeTAD (black)) measured after (a) 2 days (fresh) and (b) 3 months storage in an air filled desiccator (oxidation), (c) 3 months storage in an air filled desiccator after light soaking.

Table 1 Device characteristics for the best FTO|TiO_2|LEG4|HTM|Ag ssDSSCs from the first series (50 mg ml^{-1} TPABT, 76 mM LiTFSI and 228 mM *t*BP (S2), and 75 mM LiTFSI and 342 mM *t*BP (T3)), the second series (75 mM LiTFSI and 76 mM *t*BP and 50 mg ml^{-1} TPABT), and the Spiro-OMeTAD references (25 mM LiTFSI and 76 mM *t*BP and 100 mg ml^{-1} Spiro-OMeTAD) measured after (a) 2 days (fresh), (b) 3 months storage in an air filled desiccator (oxidation), and (c) 3 months storage in an air filled desiccator after light soaking. V_{OC} = the open circuit voltage, J_{SC} = short circuit current density, FF = fill factor, PCE = solar to electrical power conversion efficiency

	(a) Fresh sample				(b) After oxidation				(c) After light soaking			
[*t*BP] mM	V_{OC} (V)	J_{SC} (mA cm^{-2})	FF	PCE (%)	V_{OC} (V)	J_{SC} (mA cm^{-2})	FF	PCE (%)	V_{OC} (V)	J_{SC} (mA cm^{-2})	FF	PCE (%)
342 (TPABT)	0.64	0.10	0.37	0.02	0.67	4.75	0.39	1.22	0.68	4.63	0.58	1.83
228 (TPABT)	0.69	0.31	0.20	0.04	0.65	2.12	0.42	0.58	0.71	4.93	0.65	2.26
76 (TPABT)	0.68	0.21	0.33	0.05	0.70	0.95	0.49	0.33	0.73	5.11	0.40	1.48
76 (Spiro-OMeTAD)	0.82	7.05	0.68	3.78	0.88	6.89	0.43	2.49	0.84	7.14	0.53	3.03

indicating inefficient dye regeneration and high recombination, which may be more significant with TPABT because of a lower hole mobility and conductivity than Spiro-OMeTAD.[28] The *J*–*V* plots of the best cells are shown in Fig. 3a. The PCE for the best TPABT device in this series was only 0.05%.

These initial results were disappointing. However, upon remeasuring the *J*–*V* characteristics of the same solar cells after storage in a desiccator for 3 months, the PCE of the TPABT devices increased from 0.02% to *ca.* 1.2% for the best cells (Fig. 2b, 3b and Table 1). We hypothesised that the oxidation time for Spiro-OMeTAD-based ssDSSCs and TPABT-based ssDSSCs may differ due to the closer packing of TPABT molecules, driven by the intermolecular hydrogen bonding,[28] requiring more time for oxygen to penetrate through the HTM. Previously we showed that PSC were more stable with TPABT compared to Spiro-OMeTAD due to slower diffusion of oxygen and moisture through the HTM layer.[28] Alternatively, the packing of the TPABT may disrupt the stabilising interactions between the Li^+ and oxidised TPABT, slowing down charge-hopping though the film.[9]

The 3 months-old ssDSSCs were further studied during exposure to a light soaking treatment (Fig. S2–S4 and Table 1). The applied potential was cycled between open circuit (OC) and short circuit (SC) while the devices were placed under illumination from the solar simulator. Interestingly, after repeated cycling, the hysteresis was observed to decrease until it was almost negligible for all the devices. Combined with this, the J_{SC} and PCE both increased up until a certain scan number (differing for each LiTFSI concentration), at which point they stabilised. For the TPABT device with 75 mM LiTFSI and 76 mM *t*BP, the PCE increased from 0.33% to 1.48% following the light soaking treatment (Fig. 3). This behaviour was reproducible across the TPABT ssDSSCs, with the most significant enhancement consistently found for ~75 mM LiTFSI. The EQE is consistent with this increase in current (Fig. S7) for the optimum concentration of LiTFSI (75 mM). For device S2 (228 mM *t*BP, 76 mM LiTFSI) the PCE increased from 0.58% (after 3 months) to 2.26% after light soaking (Fig. 2). The observed increase in J_{SC}, FF, and V_{OC} in our devices is consistent with the mechanism hypothesised by Johannson *et al.*, where a light soaking treatment leads to Li^+ ion migration from the TiO_2 pores toward the TiO_2|dye interface. Li^+ ions screen or trap conduction band electrons after injection, inhibiting charge recombination and increasing the Fermi level of electrons in the TiO_2.[37]

The S2 and T3 devices had a better fill factor than the TPABT device with the lower concentration *t*BP (76 mM, Fig. 3), which contributed to the higher efficiency. The *t*BP may influence the concentration of cations at the TiO_2 surface and/or block charge-recombination at the TiO_2|HTM interface.[44–46] It is also reported to complex with Li^+, reducing the ionic mobility, trap density and capacitive charging/discharging that leads to

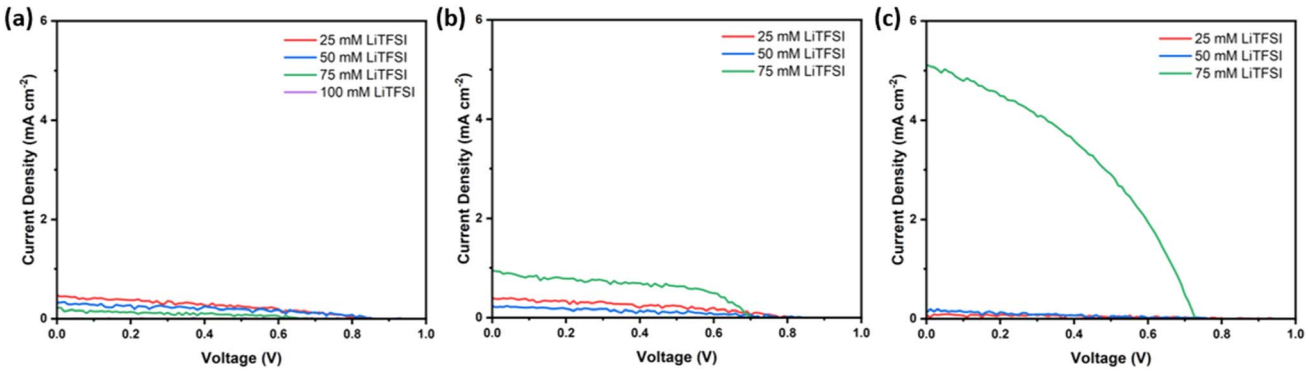

Fig. 3 *J*–*V* curves of a second series of FTO|TiO_2|LEG4|HTM|Ag ssDSSC with TPABT (76 mM *t*BP, 50 mg ml^{-1} TPABT and different concentrations LiTFSI: 25 mM (red), 50 mM (blue), 75 mM (green) and 100 mM (purple)) measured after (a) 2 days (fresh) and (b) 3 months storage in an air filled desiccator (oxidation), (c) 3 months storage in an air filled desiccator after light soaking.

hysteresis.[13,29] Johansson *et al.* observed a greater and much slower (~60 minutes *vs.* ~2 minutes) enhancement in efficiency under light soaking for the *N*,*N*,*N*′,*N*′-tetrakis(4-methoxyphenyl) benzidine (MeO-TPD) HTM compared to Spiro-OMeTAD.[37] They attributed this to hindered ion migration in the MeO-TPD due to a tighter molecular packing compared to more open structure of Spiro-OMeTAD. In their work, an improvement in efficiency with increasing LiTFSI concentration was similarly observed and this was shown to be concomitant with an increase in electron lifetime.

Optical and time-resolved spectroscopy characterisation

The semi-transparency of ssDSSCs provides an opportunity to optically probe the processes occurring in the device. UV-visible spectroscopy of the films recorded periodically over 23 days (Fig. S8 and S9) shows the steady growth of a band at *ca.* 750 nm, which is consistent with the oxidation of the triphenylamine moiety.[28,47] This feature was also present in the reflectance spectra of the complete devices (Fig. S7e) containing TPABT but not Spiro-OMeTAD. This supports our hypothesis that the oxidation in air continues over many days for TPABT on storage in an air-filled desiccator. It is known that both Li^+ and O_2 are required for Spiro-OMeTAD to be oxidised during storage and the ssDSSC to function.[48] The intensity of the feature at 750 nm in the reflectance spectra increased after light soaking (Fig. S7f).

To explore the dynamics of charge-transfer in these systems, ultrafast transient absorption spectroscopy (TAS) was performed on devices which had been left in a desiccator for 3 weeks after assembly but had not been subjected to light soaking (Fig. 4 and S14–S26). The TA spectra for TiO_2|LEG4 on a ps timescale show the characteristic bleach for the depletion of the ground state of the dye and formation of the transient absorption bands at *ca.* 450 nm and 670 nm.[49] Slight shifts within the first 10 ps are consistent with relaxation and charge-injection into TiO_2 (forming TiO_2^-|LEG4$^+$). The bands at 670 nm and 770 nm correspond to the oxidised dye and decay over the ns–μs timescale as expected. In the region between 750–800 nm, broad transient absorption is attributed to intra-band transitions of injected electrons in the TiO_2 conduction band.[49–51] The TA spectra for samples which included the spin-coated Spiro-OMeTAD HTM were quite different, even with time delays shorter than 5 ps. The bleach was less broad and the intensity of the transient absorption band at 670 nm was smaller. This is consistent with rapid charge separation – either from the dye to the HTM or from the dye to the TiO_2. The spectra agreed with the derivative of the absorption spectrum of the dye which corresponds to the "Stark shift" caused by the electric field across the interface (Spiro-OMeTAD^{+-}|LEG4|TiO_2^-).[52] The absence of the transient absorption band indicates that the ground state of LEG4 has been regenerated through electron transfer from the HTM to the oxidised dye. The spectra then ultimately decayed on a >50 μs timescale, consistent with charge-recombination between the electrons in the TiO_2 and holes in the Spiro-OMeTAD HTM.

The TAS for the films including the TPABT HTM combined features from both the HTM-free sample and the sample including Spiro-OMeTAD. Interestingly, the features were affected by the LiTFSI concentration, particularly at short (<10 ps) delay time. There was a slight (~10 nm) red shift in the transient at *ca.* 450 nm. There are slight changes in the positions of the isosbestic points on the ultrafast timescale and these are more pronounced on a ns -μs timescale, where there is a systematic red shift (~30 nm) as the LiTFSI concentration is increased. We attribute these to electronically stabilising effects of Li^+ at the dye|TiO_2 interface but note that there is also an overlap with the Stark shift caused by the electric field across the dye as charge-separation proceeds.[49,53,54] A significant increase in the intensity of this transient absorption band and a decrease in intensity of a shoulder at *ca.* 650 nm with increasing Li^+ concentration was observed. This is accompanied by an increase in intensity of the transient absorption at *ca.* 670 nm with higher concentrations of LiTFSI which is consistent with a higher concentration of oxidised dye on this short delay time. We attribute these to (1) an acceleration of charge-injection at the TiO_2|LEG4 interface due to adsorption of Li^+ at the TiO_2 surface stabilising the conduction band edge and (2) retardation of recombination on an ultrafast timescale due to charge-screening of the electrons from the oxidised dye and HTM by the Li^+.[42,55]

At the highest Li^+ concentration, a sharper absorption feature at *ca.* 700 nm was observed, which is consistent with oxidised triphenylamine.[56,57] As mentioned above, this feature is present in the wavelength-dependent reflectance spectra (Fig. S7), but it is absent in the EQE, which, instead, only matched shape of the absorption spectra of the LEG4 dye which is transparent >700 nm). This agrees with the assignment of the absorption feature as the product of TPABT oxidation, either by reaction with air or by light-induced electron transfer.[58] The presence of the oxidised HTM at such short timescales is consistent with previous studies with ssDSSCs incorporating Spiro-OMeTAD.[59] Either rapid regeneration occurs (forming TiO_2^-|LEG4|HTM$^+$) or there is an alternative reductive quenching of the excited dye by the HTM rather than oxidative quenching by the TiO_2.[53,60] The complexity of the transient absorption spectra with overlapping signals in the <100 ps timescale makes it challenging to distinguish between the two potential routes. We anticipate that increasing the LiTFSI concentration would lead to a preference for electron injection into TiO_2 rather than TPABT. The data broadly agree, since three components were required to fit the ultrafast TAS using global analysis for 25–50 mM LiTFSI but only two components were required for 75–100 mM LiTFSI (see SI). However, the increase in apparent concentration of oxidised TPABT with light soaking would be consistent with an oxidation process which does not contribute to the photocurrent (*i.e.* irreversibility). We note that the heterogeneous behaviour across all timescales of the experiment is partly complicated by the competing impacts of electron accumulation in TiO_2 (leading to a blue shift in the transient absorption of the dye) and the subsequent Li^+ accumulation at the TiO_2 surface (leading to a red shift), in addition to the likelihood that not all the pores are filled with HTM.[49] The presence of steps in the IQE spectra are consistent with incomplete pore filling.

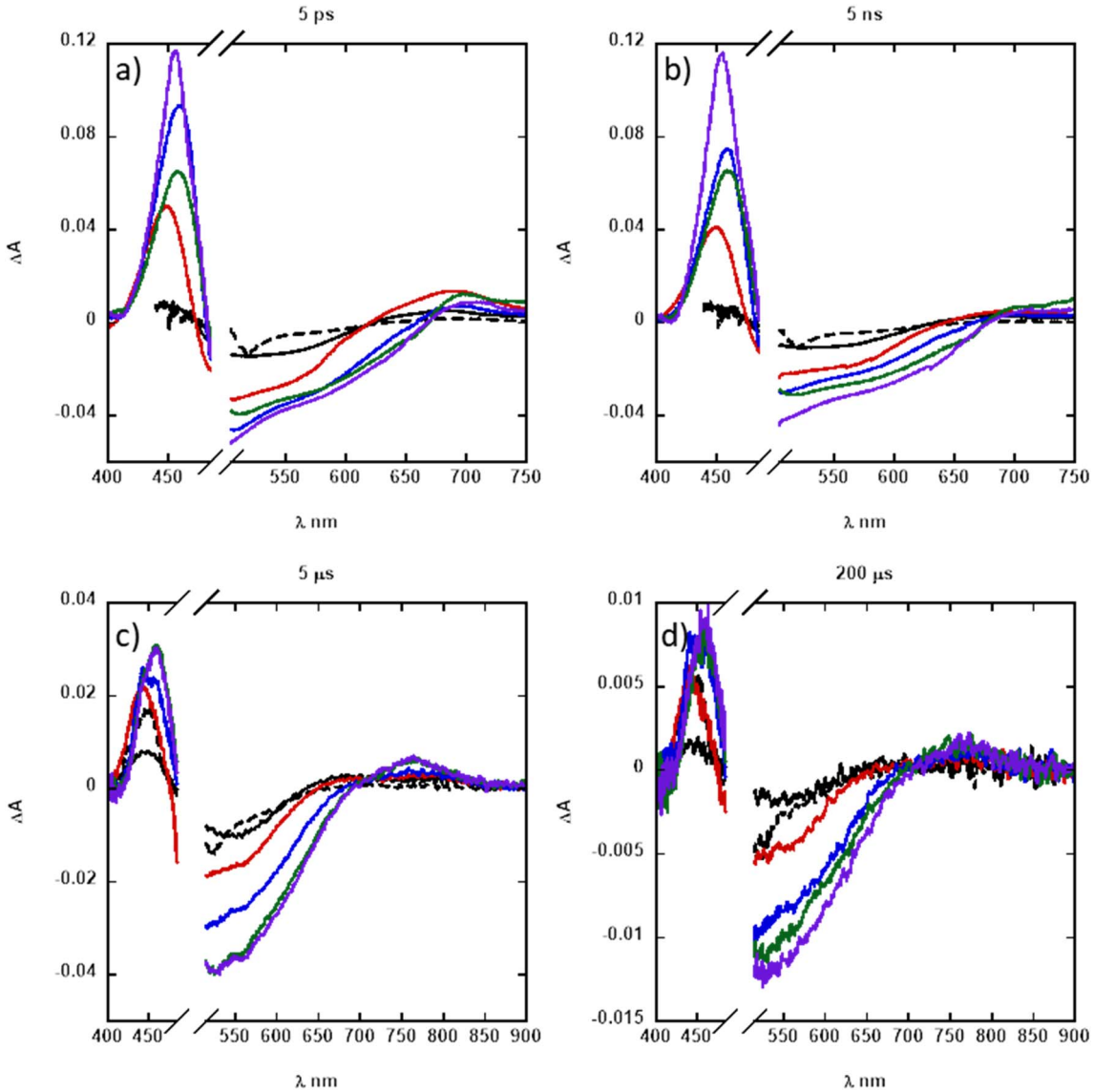

Fig. 4 Transient absorption spectra of TiO_2|LEG4 (black solid line) and TiO_2|LEG4|Spiro-OMeTAD with 25 mM LiTFSI (black dashed line) and FTO|TiO_2|LEG4|TPABT with different concentrations of LiTFSI (red = 25 mM, blue = 50 mM, green = 75 mM, purple = 100 mM) at (a) 5 ps, (b) 5 ns, (c) 5 µs, and (d) 200 µs after excitation. All samples had a *t*BP concentration of 76 mM.

For Spiro-OMeTAD, the dye regeneration was completed within 5 ns. In contrast, fairly little change in the intensity of the spectral features was observed on a ps–ns timescale for TPABT, except for a slight flattening of the transient absorption above 670 nm. By 5 µs, the spectra decayed in intensity and evolved to two groups of features. For 25 mM LiTFSI and HTM-free samples, a residual signal for the oxidised dye persisted at 670 nm, which is accompanied by a transient absorption band with a maximum at 440 nm. For high concentrations of LiTFSI, a peak at 760 nm accompanied by a transient with a maximum at 460 nm grew in, which we attribute to the oxidised TPABT, which overlapped with the Stark shift described above. There was a clear isosbestic point between the two at 710 nm. These features decay almost to the baseline in the duration of the experiment. At a time delay of 200 µs, the spectra for the high Li^+ concentration are very similar in structure and amplitude. At lower concentration of Li^+ (TPABT, Spiro and HTM-free) the spectra were similar amplitude to each other, with residual oxidised dye in absence of HTM. By the end of the experimental window, a similar residual concentration of charge-separated carriers is present. From the global analysis (Table S5), it was clear that at the same concentration (25 mM) LiTFSI, dye-regeneration with TPABPT (42.9 ps ± 4.4) was slower than with Spiro-OMeTAD (2.68 ps ± 0.31).

To further investigate how the dye-regeneration step, where charge is transferred from the HTM to the photooxidised dye, might have been affected by the different additive concentrations and degree of oxidation, photoinduced absorption (PIA) measurements were conducted by exciting the films with a 405 nm diode laser (Fig. 5 and SI, S10–S13). The PIA spectrum

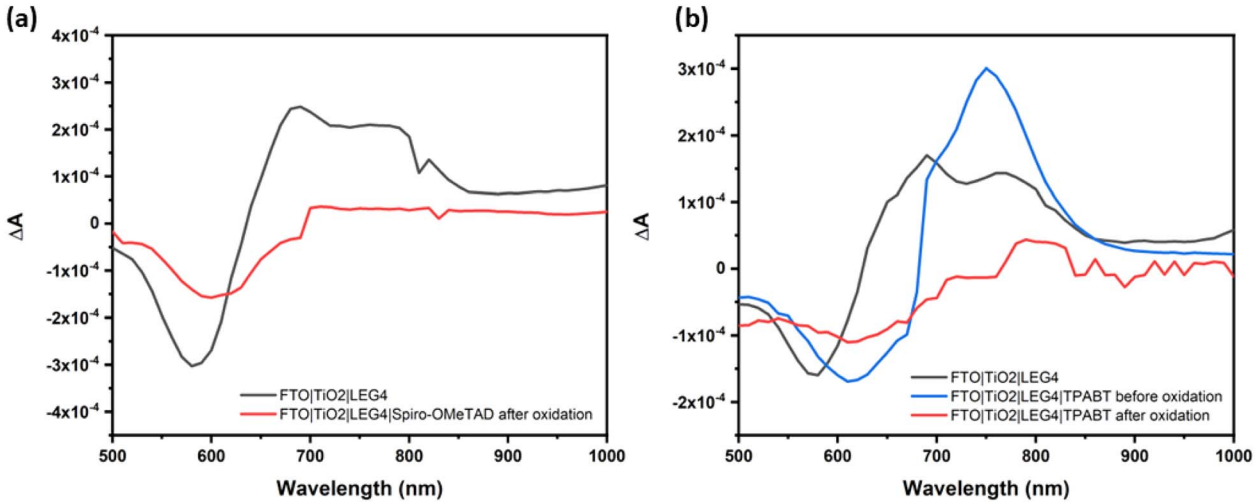

Fig. 5 (a) Photoinduced absorption spectra of FTO|TiO_2|LEG4 (black) and FTO|TiO_2|LEG4|Spiro-OMeTAD (red) after oxidation. (b) Photoinduced absorption spectra of FTO|TiO_2|LEG4 (black) and FTO|TiO_2|LEG4|TPABT (blue) before and (red) after oxidation. The HTM contained 75 mM LiTFSI, 76 mM *t*BP and 50 mg ml^{-1} TPABT.

for TPABT|TiO_2 shows no significant change in transmittance, as expected. The PIA spectrum for LEG4|TiO_2 contains a negative band (bleach) corresponding to depletion of the ground state (*ca.* 580 nm) and a positive transient absorption (*ca.* 680 nm) corresponding to the formation of the photo-oxidised dye (*i.e.* $LEG4^+|TiO_2^-$). When a layer of Spiro-OMeTAD was added, there was a red-shift of the bleach due to the presence of the HTM and additives. The spectra agreed with TAS on a μs timescale, showing the formation of Spiro-$OMeTAD^{+}$|LEG4|TiO_2^-.[52] The absence of the transient absorption band indicates that the ground state of LEG4 has been regenerated through electron transfer from the HTM to the oxidised dye.

The steady-state PIA spectra of the freshly prepared samples (Fig. S11) show a dependence of the intensity of the signal with the composition of the HTM. The signal is enhanced for TiO_2-|LEG4|TPABT with the lowest concentration of LiTFSI compared to TiO_2|LEG4, probably due to more efficient electron injection into the TiO_2 conduction band or slower charge-recombination due to enhanced trapping of the electrons at the TiO_2 interface.[52] There is a general trend that the intensity decreases with increasing concentration of LiTFSI and increasing concentration of TPABT. The latter is likely to be due to improved pore filling with the higher concentration of HTM, leading to more complete dye-regeneration. The residual signal for all samples shows that some oxidised dye remains in the μs resolution of the experiment. The amount of oxidised dye remaining is reduced when higher concentrations of LiTFSI are present.

The PIA spectra for TPABT devices measured 3 days after device fabrication (Fig. S12) show a bleach with a minimum between 600–620 nm (assigned to the loss of the ground state dye – D) and a positive absorption feature with maxima at 670 nm and 770 nm (assigned to the oxidised dye state – D^+).[30,52] This indicates that not all of the dye molecules were "regenerated" by the HTM on this timescale. For the lower concentrations of LiTFSI, the bleach at 620 nm and a transient with a maximum centred around 750 nm were more intense. This is consistent with enhanced dye regeneration. For these devices measured 23 days after fabrication (Fig. S13), a quenching of the oxidised dye state was observed for all but one concentration of additives (T5 device). This indicates that dye regeneration is more efficient for devices following a prolonged duration of oxidation.

These results are consistent with the observation that the time required for sufficient oxidation of TPABT is much longer than for Spiro-OMeTAD, which is shown to quench the oxidised dye state after only 3 days. The reason that dye-regeneration is enhanced after increasing the concentration of oxidised HTM is not obvious, but we note that the offset in potential between the HOMO of the dye and TPABT is small (the values Fig. 1 are estimates extrapolated from electrochemical experiments) and are likely to change under the different operational conditions. Kroeze *et al.* showed that additives such as LiTFSI and *t*BP affect the hole-transfer (dye-regeneration) yield in ssDSSCs with non-Spiro-OMeTAD HTMs by altering the local electrostatic interactions and energetics (including the TiO_2 density of states and the dye and HTM ionisation potentials).[44] For TPABT, we propose that there is an increase in thermodynamic driving force or a better overlap between the density of states across the interface for charge-transfer to the HTM which increases the efficiency of the dye-regeneration process.

Discussion

Our study highlights the potential for amide-based HTMs, which are straightforward to assemble and easy to modify, to replace Spiro-OMeTAD in ssDSSCs. However, TPABT oxidises slowly in air over three weeks (much slower than Spiro-OMeTAD, which oxidises in a few days) and its oxidation state strongly influences device behaviour. This prolonged oxidation alters charge-transfer and regeneration kinetics and explains time-dependent changes in device performance.

It is well understood that LiTFSI and O_2 is needed for oxidation and doping of small molecule HTMs such as Spiro-

OMeTAD.[15] Cappel *et al.* proposed that light induced processes at the TiO_2|Dye|HTM interface at the photoanode accelerate oxygen induced doping of Spiro-OMeTAD where Li^+ participates by stabilising the reduced products.[48] Previously, the polarisable amide bonds in TPABT and related HTMs were expected to facilitate a homogeneous distribution of the ions throughout the HTM due to the interactions between Li^+ ions and carbonyl oxygen.[9,61] Qi *et al.* showed that Li^+ accompanies the oxidised Spiro-OMeTAD and migrates to the opposite (Ag electrode) surface where the HTM is oxidised at the interface with air.[62] Similarly Schölin *et al.* showed, using photoelectron spectroscopy, that LiTFSI dominates at the interface between the spiro-OMeTAD film and the air/counter electrode.[17] Ageing can lead to diffusion and distribution of the LiTFSI throughout the HTM layer.[35] Others have shown the positive effect of light-soaking on device performance in PSCs where undoped HTMs are used.[63] The effect is suppressed in devices with fully optimized, doped, or heavily engineered HTMs, typically leading to a marginal response in spiro-OMeTAD. In such PSCs, the light soaking can be attributed to ion migration in the absorber layer and interfaces.[64]

TAS and PIA show that increasing LiTFSI concentration causes electronic stabilisation of the TiO_2 conduction band, indicated by the spectral shifts, increased intensity of signals assigned to the oxidised dye (especially at short delay times <10 ps), faster injection from the dye into TiO_2, and slower recombination with increasing concentration of Li^+. These findings are consistent with previous studies which show that small cation (such as Li^+) adsorption modifies conductivity/charge screening and can change fill factor/series resistance.[37] The Li^+ balances and screens the charge introduced into the TiO_2 nanoparticles following light-induced charge-transfer from the dye molecules and Li^+ adsorption shifts the TiO_2 conduction-band edge (increasing the driving force for injection) and alters the density of trap states, effects that are partly modulated by *t*BP. In ssDSSCs the situation becomes even more complicated, because the Li^+ also affects the energy of the electronic states in the HTM.[65]

The results also highlight the HTM-dependence of the dye-regeneration (Spiro-OMeTAD regenerates the dye very rapidly (approx. 2–5 ps); TPABT regenerates much more slowly (approx. 40 ps)), which, for TPABT, become more efficient with higher LiTFSI concentration and increased HTM oxidation. It has been shown that electron injection creates a local electric field at the TiO_2|Dye interface, which attracts the Li^+ ions, altering the space-charge and screening the electrons from the oxidised HTM cations.[37,66] This screening may supress charge recombination, increasing the electron lifetime, and enhance the photocurrent and solar cell performance.[46] TPABT requires substantial oxidation to reach high efficiency. Higher LiTFSI concentrations led to improved dye-regeneration (which was enhanced over *ca.* 23 days, consistent with the gradual accumulation of oxidised TPABT) and less residual oxidised dye on the μs timescale (*i.e.* more complete regeneration) and improved pore filling at high HTM loadings led to reduced recombination. Oxidation also increases conductivity of the HTM, leading to the improved device performance.[28] Too much Li^+ can increase recombination paths, however. For the highest concentration (100 mM LiTFSI), the devices did not work.

In this work, the results are consistent with the oxidation and light soaking treatments altering the distribution of the ions in the film and electric fields at the photoanode and cathode. This modulation of the energy level alignment at the interfaces affects the efficiency of charge transfer. Less recombination occurs at the dye–TiO_2 interface after oxidation and less recombination at the TiO_2|HTM interface occurs after light soaking and Li^+ migration. Spiro-OMeTAD has a fairly open structure due to the inhibition of intermolecular π–π stacking in the film. Therefore, the ions can freely move throughout the film in response to an applied electric field or change in concentration due to a chemical reaction. The close packing of TPABT may inhibit the movement of ions and oxygen through the film, leading to the slow response and substantial effects observed in this work. However, the transient absorption spectroscopy did not reveal a limitation due to the kinetics of charge injection, regeneration or recombination. The sharp features in the TAS and PIA for higher LiTFSI concentrations may indicate a localised charge-separated state. The uneven distribution of oxidised HTM and accompanying Li^+ may limit charge-transport. Before prolonged oxidation and light soaking, there may be a relative depletion of Li^+ at the photoanode surface. On prolonged oxidation and subsequent light soaking, an increase in Li^+ concentration at the photoanode surface may improve charge separation and a more consistent distribution of oxidised HTM may improve mobility through the bulk of the HTM.

Conclusions

Overall, these results highlighted that the alternative HTM, TPABT, required much longer to oxidise than state-of-the-art Spiro-OMeTAD, which was important for dye regeneration. However, the optimal oxidation time is yet to be determined. Additionally, a light soaking treatment was essential for TPABT-based ssDSSCs to minimise *J–V* hysteresis and improve PCE from 0.58% to 2.26%. Therefore, this investigation has underscored several parameters that need to be considered for new HTMs, that may not apply to the benchmark system. In future, we propose to explore these effects following accelerated doping of new HTMs through partial chemical oxidation, rather than air.[67]

Conflicts of interest

There are no conflicts to declare.

Data availability

Data supporting the findings of this study, including processed photovoltaic performance data and spectroscopic kinetic data, are available from the corresponding author upon reasonable request. Raw device and spectroscopic datasets are archived and are available through our secure, open access repository (data.ncl.ac.uk). DOI: https://doi.org/10.25405/data.ncl.30788537.

Supplementary information (SI): experimental information, device characterisation, UV-Vis, PIA, TAS and IQE. See DOI: https://doi.org/10.1039/d5ra09351a.

Acknowledgements

EAG thanks the ERC for starting grant p-TYPE 715354. Transient Absorption Spectroscopy was recorded at the North East Transient Absorption Spectroscopy and Microscopy Facility at Newcastle University EPSRC grant EP/W006340/1.

References

1 A. B. Muñoz-García, I. Benesperi, G. Boschloo, J. J. Concepcion, J. H. Delcamp, E. A. Gibson, G. J. Meyer, M. Pavone, H. Pettersson, A. Hagfeldt and M. Freitag, *Chem. Soc. Rev.*, 2021, **50**, 12450–12550.
2 M. A. Green, A. Ho-Baillie and H. J. Snaith, *Nat. Photonics*, 2014, **8**, 506–514.
3 F. Liu, T. Hou, X. Xu, L. Sun, J. Zhou, X. Zhao and S. Zhang, *Macromol. Rapid Commun.*, 2018, **39**, 1700555.
4 Z. Luo, R. Ma, T. Liu, J. Yu, Y. Xiao, R. Sun, G. Xie, J. Yuan, Y. Chen, K. Chen, G. Chai, H. Sun, J. Min, J. Zhang, Y. Zou, C. Yang, X. Lu, F. Gao and H. Yan, *Joule*, 2020, **4**, 1236–1247.
5 P. Mondelli, P. Kaienburg, F. Silvestri, R. Scatena, C. Welton, M. Grandjean, V. Lemaur, E. Solano, M. Nyman, P. N. Horton, S. J. Coles, E. Barrena, M. Riede, P. Radaelli, D. Beljonne, G. N. M. Reddy and G. Morse, *J. Mater. Chem. A Mater.*, 2023, **11**, 16263–16278.
6 R. Jones-Albertus, D. Feldman, R. Fu, K. Horowitz and M. Woodhouse, *Prog. Photovoltaics Res. Appl.*, 2016, **24**, 1272–1283.
7 M. M. Lee, J. Teuscher, T. Miyasaka, T. N. Murakami and H. J. Snaith, *Science*, 2012, **338**, 643–647.
8 U. Bach, D. Lupo, P. Comte, J. E. Moser, F. Weissörtel, J. Salbeck, H. Spreitzer and M. Grätzel, *Nature*, 1998, **395**, 583–585.
9 M. L. Petrus, K. Schutt, M. T. Sirtl, E. M. Hutter, A. C. Closs, J. M. Ball, J. C. Bijleveld, A. Petrozza, T. Bein, T. J. Dingemans, T. J. Savenije, H. Snaith and P. Docampo, *Adv. Energy Mater.*, 2018, **8**, 1801605.
10 U. Díaz and A. Corma, *Chem.–Eur. J.*, 2018, **24**, 3944–3958.
11 X. Yin, Z. Song, Z. Li and W. Tang, *Energy Environ. Sci.*, 2020, **13**, 4057–4086.
12 B. Xu, H. Tian, D. Bi, E. Gabrielsson, E. M. J. Johansson, G. Boschloo, A. Hagfeldt and L. Sun, *J. Mater. Chem. A Mater.*, 2013, **1**, 14467.
13 G. Tumen-Ulzii, T. Matsushima and C. Adachi, *Energy Fuels*, 2021, **35**, 18915–18927.
14 Z. Hawash, L. K. Ono and Y. Qi, *Adv. Mater. Interfaces*, 2018, **5**, 1700623.
15 A. Abate, T. Leijtens, S. Pathak, J. Teuscher, R. Avolio, M. E. Errico, J. Kirkpatrik, J. M. Ball, P. Docampo, I. McPherson and H. J. Snaith, *Phys. Chem. Chem. Phys.*, 2013, **15**, 2572.
16 S. N. Habisreutinger, N. K. Noel, H. J. Snaith and R. J. Nicholas, *Adv. Energy Mater.*, 2017, **7**, 1601079.
17 R. Schölin, M. H. Karlsson, S. K. Eriksson, H. Siegbahn, E. M. J. Johansson and H. Rensmo, *J. Phys. Chem. C*, 2012, **116**, 26300–26305.
18 D. Zhang, D. Li, Y. Hu, A. Mei and H. Han, *Commun. Mater.*, 2022, **3**, 58.
19 I. Lee, J. H. Yun, H. J. Son and T.-S. Kim, *ACS Appl. Mater. Interfaces*, 2017, **9**, 7029–7035.
20 H. Zhu, Z. Shen, L. Pan, J. Han, F. T. Eickemeyer, Y. Ren, X. Li, S. Wang, H. Liu, X. Dong, S. M. Zakeeruddin, A. Hagfeldt, Y. Liu and M. Grätzel, *ACS Energy Lett.*, 2021, **6**, 208–215.
21 F. M. Rombach, S. A. Haque and T. J. Macdonald, *Energy Environ. Sci.*, 2021, **14**, 5161–5190.
22 Y. Ren, D. Zhang, J. Suo, Y. Cao, F. T. Eickemeyer, N. Vlachopoulos, S. M. Zakeeruddin, A. Hagfeldt and M. Grätzel, *Nature*, 2023, **613**, 60–65.
23 M. Freitag, Q. Daniel, M. Pazoki, K. Sveinbjörnsson, J. Zhang, L. Sun, A. Hagfeldt and G. Boschloo, *Energy Environ. Sci.*, 2015, **8**, 2634–2637.
24 T. Keller, I. Benesperi, J. Thyr, T. Edvinsson, E. A. Gibson and M. Freitag, *Phys. Chem. Chem. Phys.*, 2025, **27**, 16022–16029.
25 B. Xu, D. Bi, Y. Hua, P. Liu, M. Cheng, M. Grätzel, L. Kloo, A. Hagfeldt and L. Sun, *Energy Environ. Sci.*, 2016, **9**, 873–877.
26 Y. Jang, S. Thogiti, K. Lee and J. Kim, *Crystals*, 2019, **9**, 452.
27 M. L. Petrus, T. Bein, T. J. Dingemans and P. Docampo, *J. Mater. Chem. A Mater.*, 2015, **3**, 12159–12162.
28 E. A. A. Alkhudhayr, D. Sirbu, M. Fsadni, B. Vella, B. T. Muhammad, P. G. Waddell, M. R. Probert, T. J. Penfold, T. Hallam, E. A. Gibson and P. Docampo, *ACS Appl. Energy Mater.*, 2023, **6**, 11573–11582.
29 L. Nakka, Y. Cheng, A. G. Aberle and F. Lin, *Adv. Energy Sustain. Res.*, 2022, **3**, 2200045.
30 J. Zhang, N. Vlachopoulos, M. Jouini, M. B. Johansson, X. Zhang, M. K. Nazeeruddin, G. Boschloo, E. M. J. Johansson and A. Hagfeldt, *Nano Energy*, 2016, **19**, 455–470.
31 B. Xu, J. Huang, H. Ågren, L. Kloo, A. Hagfeldt and L. Sun, *ChemSusChem*, 2014, **7**, 3252–3256.
32 B. Xu, E. Gabrielsson, M. Safdari, M. Cheng, Y. Hua, H. Tian, J. M. Gardner, L. Kloo and L. Sun, *Adv. Energy Mater.*, 2015, **5**, 1402340.
33 W. Yang, N. Vlachopoulos, Y. Hao, A. Hagfeldt and G. Boschloo, *Phys. Chem. Chem. Phys.*, 2015, **17**, 15868–15875.
34 M. G. Helander, M. T. Greiner, Z. B. Wang, W. M. Tang and Z. H. Lu, *J. Vac. Sci. Technol.*, 2011, **29**, 011019.
35 Z. Zhang, Z. Li, L. Deng, Y. Gao, C. Wang, J. Xu, T. Li and P. Gao, *ACS Appl. Mater. Interfaces*, 2022, **14**, 4378–4388.
36 Y. Dong, F. M. Rombach, G. Min, H. J. Snaith, C.-T. Lin, S. A. Haque and T. J. Macdonald, *Mater. Sci. Eng. R Rep.*, 2025, **162**, 100875.
37 L. Yang, B. Xu, D. Bi, H. Tian, G. Boschloo, L. Sun, A. Hagfeldt and E. M. J. Johansson, *J. Am. Chem. Soc.*, 2013, **135**, 7378–7385.
38 L. Yang, R. Lindblad, E. Gabrielsson, G. Boschloo, H. Rensmo, L. Sun, A. Hagfeldt, T. Edvinsson and

E. M. J. Johansson, *ACS Appl. Mater. Interfaces*, 2018, **10**, 11572–11579.
39 R. Katoh, M. Kasuya, S. Kodate, A. Furube, N. Fuke and N. Koide, *J. Phys. Chem. C*, 2009, **113**, 20738–20744.
40 F. Lamberti, T. Gatti, E. Cescon, R. Sorrentino, A. Rizzo, E. Menna, G. Meneghesso, M. Meneghetti, A. Petrozza and L. Franco, *Chem*, 2019, **5**, 1806–1817.
41 P. Docampo, S. Guldin, T. Leijtens, N. K. Noel, U. Steiner and H. J. Snaith, *Adv. Mater.*, 2014, **26**, 4013–4030.
42 J. R. Jennings and Q. Wang, *J. Phys. Chem. C*, 2010, **114**, 1715–1724.
43 B. Roose, S. Pathak and U. Steiner, *Chem. Soc. Rev.*, 2015, **44**, 8326–8349.
44 J. E. Kroeze, N. Hirata, L. Schmidt-Mende, C. Orizu, S. D. Ogier, K. Carr, M. Grätzel and J. R. Durrant, *Adv. Funct. Mater.*, 2006, **16**, 1832–1838.
45 G. Boschloo, L. Häggman and A. Hagfeldt, *J. Phys. Chem. B*, 2006, **110**, 13144–13150.
46 J. Krüger, R. Plass, L. Cevey, M. Piccirelli, M. Grätzel and U. Bach, *Appl. Phys. Lett.*, 2001, **79**, 2085–2087.
47 H. Lin and G. Liou, *J. Polym. Sci. A Polym. Chem.*, 2009, **47**, 285–294.
48 U. B. Cappel, T. Daeneke and U. Bach, *Nano Lett.*, 2012, **12**, 4925–4931.
49 W. Yang, Y. Hao, N. Vlachopoulos, A. I. K. Eriksson and G. Boschloo, *J. Phys. Chem. C*, 2016, **120**, 22215–22224.
50 G. Boschloo and D. Fitzmaurice, *J. Phys. Chem. B*, 1999, **103**, 2228–2231.
51 U. B. Cappel, S. M. Feldt, J. Schöneboom, A. Hagfeldt and G. Boschloo, *J. Am. Chem. Soc.*, 2010, **132**, 9096–9101.
52 W. Yang, M. Pazoki, A. I. K. Eriksson, Y. Hao and G. Boschloo, *Phys. Chem. Chem. Phys.*, 2015, **17**, 16744–16751.
53 U. B. Cappel, A. L. Smeigh, S. Plogmaker, E. M. J. Johansson, H. Rensmo, L. Hammarström, A. Hagfeldt and G. Boschloo, *J. Phys. Chem. C*, 2011, **115**, 4345–4358.
54 W. Yang, N. Vlachopoulos and G. Boschloo, *ACS Energy Lett.*, 2017, **2**, 161–167.
55 A. Furube, R. Katoh, K. Hara, T. Sato, S. Murata, H. Arakawa and M. Tachiya, *J. Phys. Chem. B*, 2005, **109**, 16406–16414.
56 Z. Shen, B. Xu, P. Liu, Y. Hu, Y. Yu, H. Ding, L. Kloo, J. Hua, L. Sun and H. Tian, *J. Mater. Chem. A Mater.*, 2017, **5**, 1242–1247.
57 M. Ayaz, J. Khan Kasi, A. Khan Kasi, M. Bokhari and G. Boschloo, *ACS Appl. Energy Mater.*, 2022, **5**, 4240–4246.
58 G. Y. Margulis, B. E. Hardin, I. Ding, E. T. Hoke and M. D. McGehee, *Adv. Energy Mater.*, 2013, **3**, 959–966.
59 U. Bach, Y. Tachibana, J.-E. Moser, S. A. Haque, J. R. Durrant, M. Grätzel and D. R. Klug, *J. Am. Chem. Soc.*, 1999, **121**, 7445–7446.
60 S. S. K. Raavi, P. Docampo, C. Wehrenfennig, M. J. P. Alcocer, G. Sadoughi, L. M. Herz, H. J. Snaith and A. Petrozza, *J. Phys. Chem. C*, 2014, **118**, 16825–16830.
61 C. R. Kemnitz and M. J. Loewen, *J. Am. Chem. Soc.*, 2007, **129**, 2521–2528.
62 Z. Hawash, L. K. Ono, S. R. Raga, M. V. Lee and Y. Qi, *Chem. Mater.*, 2015, **27**, 562–569.
63 M. Franckevičius, A. Mishra, F. Kreuzer, J. Luo, S. M. Zakeeruddin and M. Grätzel, *Mater. Horiz.*, 2015, **2**, 613–618.
64 K. Domanski, B. Roose, T. Matsui, M. Saliba, S.-H. Turren-Cruz, J.-P. Correa-Baena, C. R. Carmona, G. Richardson, J. M. Foster, F. De Angelis, J. M. Ball, A. Petrozza, N. Mine, M. K. Nazeeruddin, W. Tress, M. Grätzel, U. Steiner, A. Hagfeldt and A. Abate, *Energy Environ. Sci.*, 2017, **10**, 604–613.
65 M. F. Aygüler, A. G. Hufnagel, P. Rieder, M. Wussler, W. Jaegermann, T. Bein, V. Dyakonov, M. L. Petrus, A. Baumann and P. Docampo, *ACS Appl. Mater. Interfaces*, 2018, **10**, 11414–11419.
66 G. Redmond and D. Fitzmaurice, *J. Phys. Chem.*, 1993, **97**, 1426–1430.
67 W. H. Nguyen, C. D. Bailie, E. L. Unger and M. D. McGehee, *J. Am. Chem. Soc.*, 2014, **136**, 10996–11001.